Asymmetric photoelectron momentum distribution driven by two-color XUV fields

Wan-Yang Wu and Feng He*

Key Laboratory for Laser Plasmas (Ministry of Education) and Department of Physics and Astronomy, Collaborative Innovation Center of IFSA (CICIFSA), Shanghai Jiao Tong University, Shanghai 200240, China

(Received 9 December 2015; published 12 February 2016)

The photoionization of He^+ in two-color XUV fields is studied by numerically solving the time-dependent Schrödinger equation. He^+ may be ionized by directly absorbing one high-energetic photon or by absorbing two photons sequentially by mediating an excited state. The interference of these two pathways results in either enhancement or suppression of photoionization, depending on the propagating direction of the photoelectron and the relative phase of two pulses. The two-pathway interference also induces the split of photoelectron momenta. This study shows that the participation of intermediate states may substantially change photoionization processes.

DOI: 10.1103/PhysRevA.93.023415

I. INTRODUCTION

Photoelectrons emitted from targets played an extremely important role in physics: it boosted the development of quantum mechanics. After the advent of laser, photoionization became a central topic in atomic and molecular physics [1]. The understanding of photoionization developed from the Einstein photoelectric effect, multiphoton ionization [2,3], above-threshold ionization [4,5], tunneling ionization [6–8], and rescattering ionization [9,10]. Molecular ionization has been used to demonstrate the Young's double-slit interference [11–14] and Fraunhofer-like diffraction [15], as well as to retrieve molecular vibration [16] and valence electron orbitals [17].

Atomic and molecular ionization in strong laser fields has been understood based on the Keldysh parameter [18], $\gamma = \sqrt{I_p/2U_p}$, where I_p is the ionization potential and U_p is the ponderomotive energy, which is the averaged quiver kinetic energy of a free electron in a laser electric field. When $\gamma \gg 1$, the laser period is much shorter than the typical time scale for the electron movement; thus, the electron sees a fast oscillating field and absorbs photons to get released from its parent ion. On the other hand, when $\gamma \ll 1$, the electron sees a very slow oscillating electric field, and thus it has enough time to adapt to the laser-distorted Coulomb potential and tunnel through the Coulomb barrier. The tunneling ionized electron may return back and rescatter with its parent ion, and its residual kinetic energy may transform into high-order harmonics [19,20]. The returning electron may also rescatter other electrons if there are any, resulting in the double or triple ionization [9,21,22].

Intermediate states play an important role in photoionization [23–25]. For an atom exposed to a combined ultraviolet attosecond and infrared femtosecond pulse, the ac Stark-shifted intermediated energy levels may be resonantly or nonresonantly reached by absorbing the ultraviolet photon. Thus, the population of the excited state as well as the ionization probability will oscillate with the time delay between the two pulses [26]. Johnsson *et al.* [27] first demonstrated that the ionization probability of helium atoms oscillates with the time delay between an attosecond pulse train and an infrared laser pulse. However, such an oscillation will not happen in argon atoms in the same laser condition because no intermediates are involved. A similar phenomenon was also observed in double ionization [28]. The ac Stark shift in attosecond time scales has been observed in the experiment [29]. Using an interferometric pump-probe technique, Mauritsson *et al.* were able to determine which states are excited by the attosecond pulse [30].

In this paper, we studied the ionization of He^+ in a two-color ($\omega_1 < \omega_2$) XUV laser field, where ω_1 and ω_2 are the XUV frequencies. The ionization of He^+ may undergo the following two pathways. He^+ is directly ionized from the ground state by absorbing a high energetic photon ω_2, and the released electron takes the energy $\omega_2 - I_p$. Alternatively, the bound electron may be indirectly ionized by first absorbing one ω_1 and reaching the first excited state before it is kicked off by absorbing another ω_1. When $\omega_2 \sim 2\omega_1$, the two ionization pathways give similar photoelectron energies. Thus, these two ionization pathways will interfere with each other, resulting in abundant structures in the photoelectron momentum distributions.

The rest of the paper is organized as follows. In Sec. II, we introduce numerical simulation methods. Section III presents numerical results as well as the analytical results from the time-dependent perturbation theory. We end the paper with the summary in Sec. IV.

II. NUMERICAL MODELS

We used He^+ as the prototype in this study. However, we point out that the interference of the direct and indirect ionization pathways is a general scenario if these two pathways give the same photoelectron energies. The ionization of He^+ in strong laser fields is governed by the time-dependent Schrödinger equation (TDSE) (atomic units are used throughout unless stated otherwise)

$$i\frac{\partial}{\partial t}\Psi(\mathbf{r};t) = \left[-\frac{1}{2}\nabla_{\mathbf{r}}^2 + V(\mathbf{r}) + \mathbf{r}\cdot\mathbf{E}(t)\right]\Psi(\mathbf{r};t), \quad (1)$$

where $\mathbf{E}(t)$ is the laser electric field and $V(\mathbf{r})$ is the Coulomb potential. Though such a three-dimensional TDSE can give precise results, it is quite time consuming. In many cases, a simplified one-dimensional model can present the main physical pictures quickly and make the data analysis eas-

*fhe@sjtu.edu.cn

ier. Therefore, in the following calculations, we first ran one-dimensional TDSE and grasped the main mechanisms before going into detailed data analysis. In a simplified one-dimensional case, we replaced $\mathbf{r}$ with x, and expressed the Coulomb potential as $V(x) = -\frac{1}{\sqrt{s_1+x^2}}$ with the soft-core parameter $s_1 = 0.062$ for obtaining the ground-state energy -2 a.u. In simulations, we set the spatial grid $\Delta x = 0.2$ a.u. and the time step $\Delta t = 0.1$ a.u. The simulation box covers the area $x \subset [-300,300]$ a.u., which is big enough to hold all ionized wave packets during the whole calculations. We also ran two-dimensional TDSE simulations for obtaining more realistic photoelectron momentum distributions, in which we expressed $V(x,y) = -\frac{1}{\sqrt{s_2+x^2+y^2}}$ with $s_2 = 0.161$. The two-dimensional simulation box is sampled by 3000×3000 grids and we set $\Delta x = \Delta y = 0.2$ a.u. The initial state was obtained by propagating the field-free Schrödinger equation in imaginary time [31], and the wave function was propagated using the Crank-Nicholson method [32].

We studied the few-photon ionization of He^+ in a two-color strong XUV field. The laser field, in two-dimensional simulations, is written as

$$E(t) = E_1 f_1(t)\mathrm{Re}[\vec{\mathbf{e}}_1 e^{i\omega_1 t}] + E_2 f_2(t)\mathrm{Re}[\vec{\mathbf{e}}_2 e^{i\omega_2(t+\phi)}], \quad (2)$$

with a Gaussian envelope $f_j(t) = e^{-4\ln 2(t/\tau_j)^2}$, where $\tau_1 = 10T_1$ and $\tau_2 = 20T_2$, with T_1 and T_2 being the periods. ϕ is the relative phase; E_1 and E_2 are two amplitudes. For the jth pulse ($j = 1,2$), the polarization vector is $\vec{\mathbf{e}}_j = (\hat{\mathbf{e}}_x + i\epsilon_j\hat{\mathbf{e}}_y)/\sqrt{(1+\epsilon_j^2)}$, where ϵ_j is the ellipticity ($0 \leqslant \epsilon_j \leqslant 1$), and $\hat{\mathbf{e}}_x$ and $\hat{\mathbf{e}}_y$ are the major and minor axes of the polarization ellipse. In one-dimensional simulations, $\epsilon_1 = \epsilon_2 = 0$, the laser field is expressed as

$$E(t) = E_1 f_1(t)\cos(\omega_1 t) + E_2 f_2(t)\cos(\omega_2 t + \phi). \quad (3)$$

To calculate the eigenstate energies, we started with a guessing wave function $\Psi(t = 0)$ and propagated it under the interaction of the field-free Hamiltonian. We recorded the autocorrelation function $a(t) = \langle\Psi(t)|\Psi(t = 0)\rangle$, and Fourier transformed $a(t)$, which gave the eigenstate energies. In the one-dimensional model, the two lowest eigenstate energies are $E_i = -2$ a.u. and $E_m = -0.93$ a.u., and for the two-dimensional model, the two lowest eigenstate energies are $E_i = -2$ a.u. and $E_m = -0.74$ a.u. In the case $\omega_1 = \Delta E = E_m - E_i$, He^+ is resonantly excited from the ground state to the first excited state by absorbing one ω_1. In later calculations, we fixed $\omega_2 = 2\Delta E$ and scanned ω_1 around ΔE.

Since the direct and indirect ionization are one- and two-photon processes, they can be alternatively studied using the time-dependent perturbation theory. The perturbation theory is helpful to disentangle different contributions in the dynamical processes. For the ionization triggered by absorbing one ω_2, the transition amplitude can be described by the first-order perturbation theory. In the two-photon process, the ionization of He^+ is mediated by the first excited state of He^+. Such an indirect ionization can be described by the second-order perturbation theory. The first- and second-order transition amplitudes are written as

$$c_1(p) = -i\mu_{f1}(p)\int_{-T/2}^{T/2} e^{i\triangle_{f1}t}E(t)dt, \quad (4)$$

$$c_2(p) = -\mu_{f2}(p)\mu_{21} \times \int_{-T/2}^{T/2} e^{i\triangle_{f2}t}E(t)\left[\int_{-T/2}^{t} e^{i\triangle_{21}t'}E(t')dt'\right]dt, \quad (5)$$

where T is the duration of laser field $E(t)$, $\triangle_{jk}$ is the energy difference between states $|j\rangle$ and $|k\rangle$, and μ_{jk} is the transition dipole. States $|1\rangle$,$|2\rangle$, and $|f\rangle$ represent the ground state, the first excited state, and the final continuum state.

The partial ionization probability is obtained,

$$\begin{aligned} W &= \int_a^b |c_1(p) + c_2(p)|^2 dp \\ &= \int_a^b |c_1(p)|^2 dp + \int_a^b |c_2(p)|^2 dp \\ &\quad + 2\mathrm{Re}\left(\int_a^b c_1^*(p)c_2(p)dp\right), \end{aligned} \quad (6)$$

by setting $[a,b]$ in different regions. For example, to calculate the ionization probabilities for electrons having momenta $p < 0$ and $p > 0$, we set $[a,b] = [-\infty,0]$ and $[0,+\infty]$, respectively. The last term in Eq. (6) indicates the interference between the direct and indirect ionization pathways.

III. SIMULATION RESULTS

A. Photoionization calculated with the one-dimensional model

As known, the relative phase between the two laser pulses plays an important role in photoionization. The symmetry of the combined field is broken for some relative phases, resulting in asymmetric photoelectron emission [33–36] or even and odd high harmonics [37]. For simplicity, we first look at the photoionization with a one-dimensional model. Figures 1(a) and 1(b) show the combined laser electric fields when the relative phase $\phi = 0$ and π, respectively. The two laser pulses have intensities $I_1 = 5 \times 10^{13}$ W/cm^2 and $I_2 = 3 \times 10^{13}$ W/cm^2. The ionization probabilities triggered by only I_1 or I_2 are almost same. Figure 1(c) shows the photoelectron momentum distribution with respect to the relative phase between the two fields. One may see that the photoelectron momentum distribution periodically changes with ϕ. The similar carrier-envelope phase (CEP)-dependent photoelectron momenta have been analyzed by others [25,38,39]. However, if the first excited state is projected out in the whole calculations, the photoelectron momentum distribution will be symmetric, as shown in Fig. 1(d). Without the first excited state, the indirect two-photon ionization can be neglected. We thus demonstrate that the intermediate states are important in photoionization.

To investigate how the first excited state takes part in the photoionization, we fixed $\omega_2 = 2\Delta E$ and scanned ω_1 around ΔE. The photoelectron momentum spectrum is shown in Fig. 2(c). It clearly shows that the photoelectron spectra have the left-right symmetry if ω_1 is very different from ΔE. In this case, ω_1 cannot induce the resonant excitation; hence the first excited state actually does not participate in the

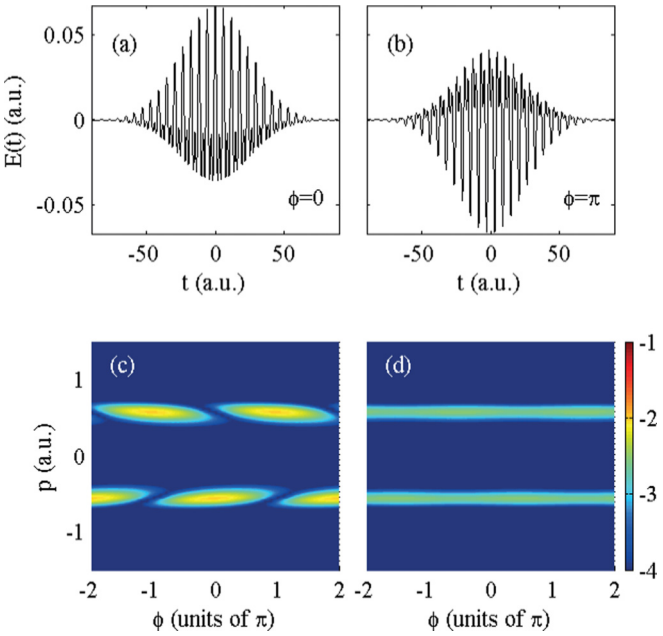

FIG. 1. The combined two-color XUV field at (a) $\phi = 0$ and (b) $\phi = \pi$. (c),(d) The photoelectron momentum distributions as a function of ϕ when the first excited state is included or projected out, respectively. The laser parameters are $\omega_1 = \Delta E = 1.07$ a.u. and $\omega_2 = 2\Delta E = 2.14$ a.u. Laser intensities are $I_1 = 5 \times 10^{13}$ W/cm^2 and $I_2 = 3 \times 10^{13}$ W/cm^2. Both pulses are linearly polarized, i.e., $\epsilon_1 = \epsilon_2 = 0$.

ionization process. Since the direct two-ω_1 ionization from the ground state is negligible, all of the ionization signals are triggered by absorbing one ω_2, and the left-right symmetry is preserved. When ω_1 approaches ΔE, the first excited state involves in the ionization process, and the very asymmetric photoelectron momentum distribution appears. The lineout

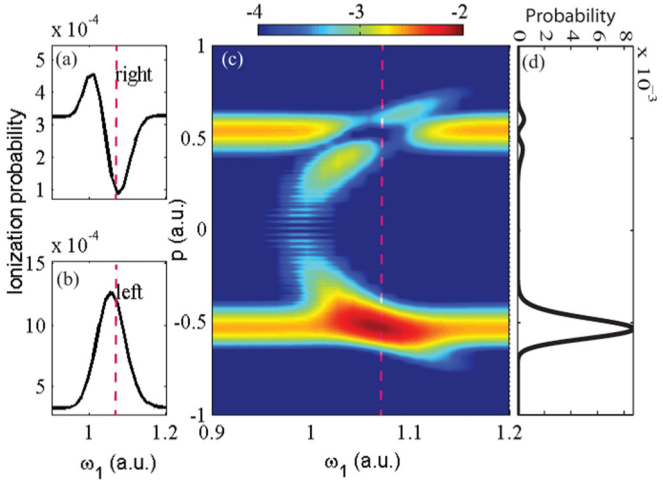

FIG. 2. (a),(b) The left- and right-going photoelectron probabilities as a function of ω_1. (c) The photoelectron momentum distribution as a function of ω_1 in the logarithmic scale. (d) The lineout of the photoelectron momentum distribution at $\omega_1 = \Delta E$ [indicated by the vertical red dashed line in (c)]. Other parameters are the same as those in Fig. 1.

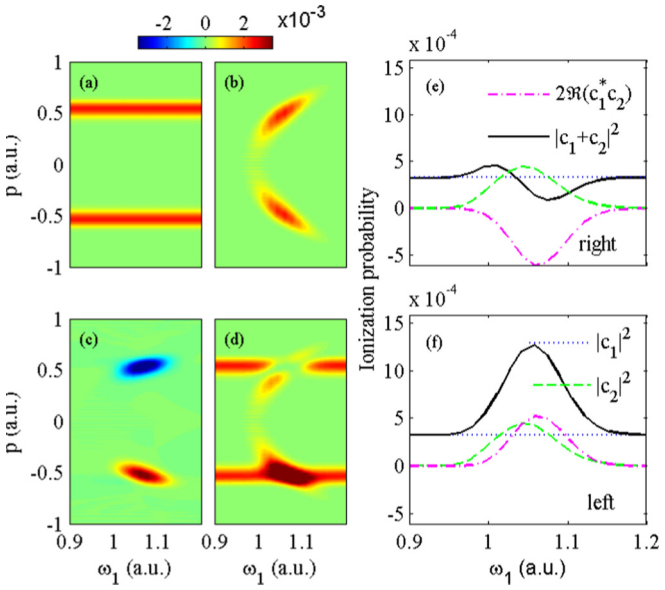

FIG. 3. (a) $|c_1(p)|^2$, (b) $|c_2(p)|^2$, (c) $2\mathrm{Re}[c_1(p)^* c_2(p)]$, (d) $|c_1(p) + c_2(p)|^2$ as a function of ω_1 in linear scale. (e),(f) Ionization probabilities of the right- and left-going electron as a function of ω_1.

of the photoelectron spectrogram at $\omega_1 = \Delta E$ is shown in Fig. 2(d). The photoelectron momentum spectrum is split and substantially suppressed when p is positive. The split of the photoelectron spectra has been explored in the field-modified Fano resonance [40,41]. By integrating the photoelectron distribution in half spaces $p > 0$ and $p < 0$, we obtained the ω_1-dependent ionization probabilities emitting along the right $(+x)$ and left $(-x)$ directions, as shown in Figs. 2(a) and 2(b), respectively. Both curves are asymmetric with respect to the dashed line.

All results in Fig. 2 can be approximately reproduced by the time-dependent perturbation theory, which can disentangle different contributions in the ionization process. Figure 3 unfolds contributions of one-photon ionization $|c_1(p)|^2$ [Fig. 3(a)], two-photon ionization $|c_2(p)|^2$ [Fig. 3(b)], and the two-pathway interference $2\mathrm{Re}[c_1(p)^* c_2(p)]$ [Fig. 3(c)] as a function of ω_1. Obviously, $|c_1(p)|^2$ has no dependence on ω_1 and shows the left-right symmetry. For the two-photon indirect ionization process, the photoelectron momentum is centered at $p = \pm\sqrt{2(\omega_1 + \Delta E - I_p)}$, thus the ω_1-dependent $|c_2(p)|^2$ has a parabolic shape. The individual contribution from the only two-photon process is also left-right symmetric. The left-right symmetry is broken in the cross term, as shown in Fig. 3(c). Such asymmetry is fundamentally originated from the transition dipoles $\mu_{f1}(p)$ and $\mu_{f2}(p)$, which carry different phases for left or right emission electrons. The addition of Figs. 3(a)–3(c) yields Fig. 3(d), which is almost identical to Fig. 2(c). The destructive and constructive interferences shown in Fig. 3(c) explain the suppression and enhancement of the ionization on both sides. One may expect that if the relative phase is reversed by π, the constructive and destructive interference will also reverse, which has been shown in Fig. 1(c) by the numerical results.

After integrating the positive and negative momentum components in Figs. 3(a)–3(d), we have the probabilities for

the left- and right-going photoelectrons as a function of ω_1, as shown in Figs. 3(e) and 3(f), respectively. For those $p > 0$, the ionization probability curve has an asymmetric shape when ω_1 sweeps over ΔE. On the other hand, for the left-going photoelectron, the maximum does not appear at $\omega_1 = \Delta E$. The minimum or maximum of the interference term $2\mathrm{Re}(c_1^* c_2)$ is not coincident with the position of the maximum of $|c_2|^2$. Remember that $|c_1|^2$ is independent of ω_1. Such results indicate that the relative phase between c_1 and c_2 plays a role in the photoionization. The phase shift between c_1 and c_2 may be understood as follows. For the one-photon process, the electron is ionized immediately once it absorbs a ω_2. For the two-photon process, He^+ is first excited to the intermediate state, and stays in the excited state for a while before it is ionized by absorbing the second ω_1. The excited He^+ acquires a phase lag in such a sequential two-photon process. This phase lag has also been discussed in [42–44].

B. Photoionization in circularly polarized XUV fields with the two-dimensional model

In the one-dimensional model, the electron movement is confined along the laser polarization direction. However, in the two-dimensional or three-dimensional model, the one- and two-photon ionization will yield photoelectrons having different spatial distributions. Therefore, it is worth looking into the direct-indirect interference in higher-dimensional calculations.

We study the ionization of He^+ in two XUV pulses which are both right-circularly polarized. Figure 4 shows the electron wave functions in position (upper) and momentum (lower) representations, and different columns are obtained by using different relative carrier-envelope phases ϕ. By scanning ϕ, the ionized electron wave-function distributions in both representations rotate accordingly. The interference of the indirect and direct ionization pathways results in the enhancement and suppression of ionization rates in two

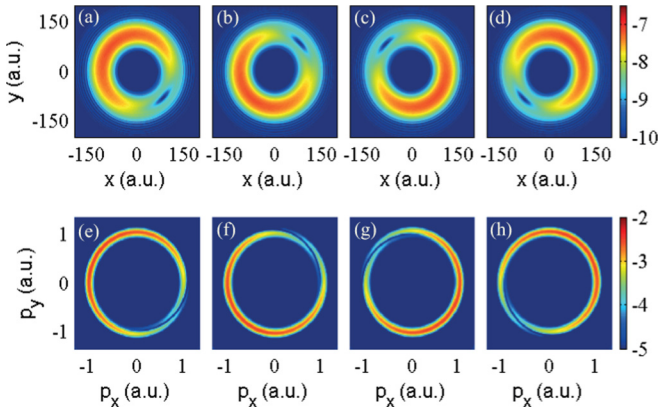

FIG. 4. The photoelectron wave functions in space (upper row) and momentum (lower row) representations. The four columns from left to right are for $\phi = 0, 0.5\pi, \pi, 1.5\pi$, respectively. Laser frequencies are $\omega_1 = \Delta E = 1.26$ a.u., $\omega_2 = 2\Delta E = 2.52$ a.u., and intensities are $I_1 = 5 \times 10^{13}$ W/cm^2 and $I_2 = 2 \times 10^{13}$ W/cm^2. Pulse durations τ_1 is $10T_1$ and τ_2 is $20T_2$. Both pulses are right-circularly polarized.

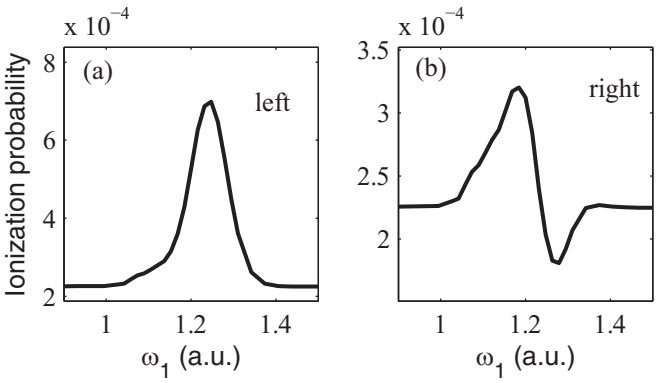

FIG. 5. The (a) left- and (b) right-going photoelectron probabilities as a function of ω_1 calculated with the two-dimensional model. Other laser parameters are the same as those in Fig. 4.

opposite quadrants. The photoelectron momentum spectra are split in the areas where the ionization is suppressed.

According to the one-dimensional calculations, the directional ionization probability may change if ω_1 sweeps over ΔE. This phenomenon still exists in two-dimensional calculations. In Figs. 5(a) and 5(b), we plotted the ionization probabilities for electrons having $p_x < 0$ and $p_x > 0$, respectively. Here, the relative phase between two XUV fields was fixed at $\phi = \pi/4$. The line shapes are very similar to those in Figs. 2(a) and 2(b). One may expect that similar results can be obtained in three-dimensional simulations.

If the two circularly polarized laser vectors rotate oppositely, the photoionization presents different characters [45]. Figure 6 shows the same snapshots as Fig. 4 but for the case that the pair of XUV pulses are left-right circularly polarized. Three minima are observed in the band for the ionized wave function in each panel, and the corresponding momentum spectrum splits when the ionization is most suppressed.

C. Rabi oscillation and two-pathway interference

For the indirect ionization process, the scenario becomes more complex if the XUV pulse having the frequency ω_1 is stronger and/or longer enough to trigger Rabi oscillation between the ground and first excited states of He^+. Rabi

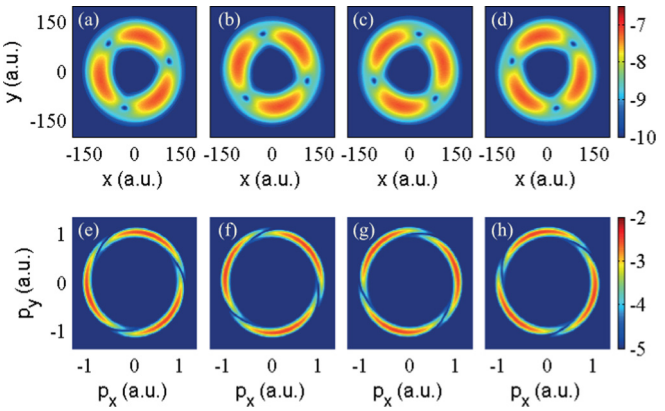

FIG. 6. Same as Fig. 4, except that the two circularly polarized XUV fields rotate oppositely, i.e., $\epsilon_1 = -\epsilon_2 = -1$.

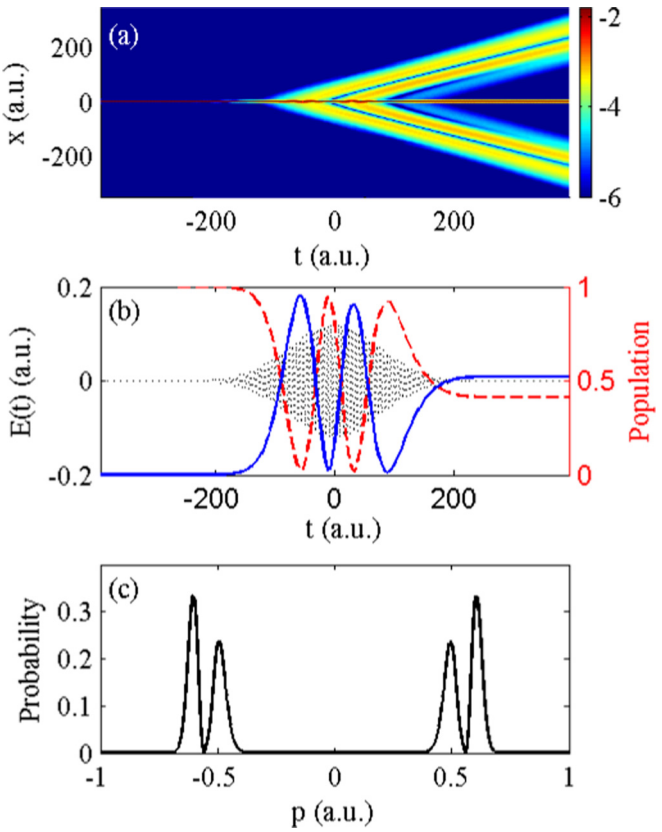

FIG. 7. (a) The time-dependent electron wave-function distribution. (b) The time-dependent probabilities for the ground state (red dashed curve) and first excited states (blue solid curve). For reference, the one-color XUV field (ω_1) is presented with the black dotted curve. (c) The photoelectron momentum distribution. The laser frequency is $\omega_1 = \Delta E = 1.07$ a.u. and the intensity is $I_1 = 5 \times 10^{14}$ W/cm^2. The pulse duration is $30T_1$,$\epsilon_1 = 0$.

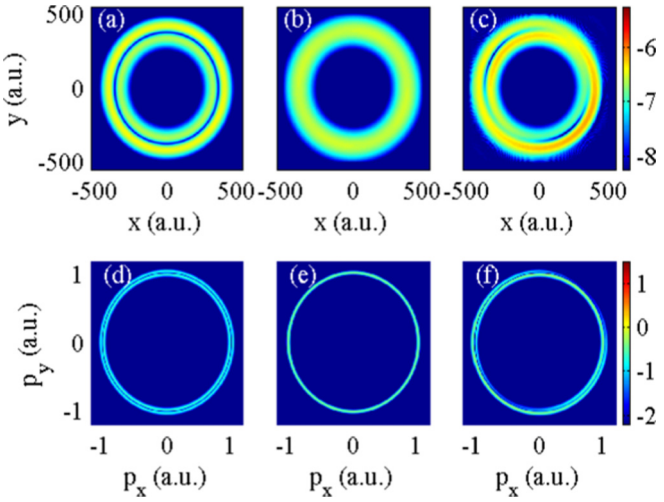

FIG. 8. (a) Photoelectron wave functions in the space (upper row) and momentum (lower row) representations. (a),(d) Only ω_1 is used; (b),(e) only ω_2 is used; (c),(f) both ω_1 and ω_2 are used. Laser parameters: $\omega_1 = \Delta E = 1.26$ a.u., $I_1 = 5 \times 10^{14}$ W/cm^2, $I_2 = 1.2 \times 10^{15}$ W/cm^2, $\tau_1 = \tau_2 = 30T_1$, $\epsilon_1 = \epsilon_2 = 1$, $\phi = 0$.

oscillation may also induce the split of photoelectron momentum spectra [46]. Because of a much longer pulse used in this section, we used a simulation box with 6000 × 6000 grids to hold all outgoing electron wave packets.

First, we solved the one-dimensional TDSE using a one-color XUV pulse with frequency $\omega_1 = \Delta E$, pulse duration $30T_1$, and laser intensity 5×10^{14} W/cm^2. Figures 7(a) and 7(b) show the time evolution of the electron wave function and the probabilities for the ground (red dashed curve) and first excited (blue solid curve) states of He^+. With the time evolution, the electron hops between the ground and first excited states. This hopping frequency depends on the laser intensity and frequency. At the moment that the population in the first excited state is large, the temporary ionization rate is large. In contrast, when the electron is dumped to the ground state, the temporary ionization rate is suppressed. This fact explains the minimum that appeared in the ejected electron wave function in Fig. 7(a). Close to the end of the laser pulse, the population of the first excited state increases, which leads to the third outgoing ejection in Fig. 7(a) but with much smaller probabilities compared to the other two ejections. We Fourier transformed the photoelectron wave packet at the end of the calculations and obtained the photoelectron momentum spectrum, which is plotted in Fig. 7(c). The Rabi oscillation results in the split of the photoelectron momentum. The separation between the two peaks is about 0.062 a.u., and the corresponding frequency equates to the Rabi frequency. With an even longer and/or stronger XUV pulse, the electron may hop between the ground and first excited states more times; thus the photoelectron momentum spectra will show multiple peaks.

We now study the interference between direct and indirect ionization pathways with a two-dimensional model when the Rabi oscillation is involved. Figure 8 shows the electron wave functions in the space (upper row) and momentum (lower row) representations. The left and middle columns are the results by only using $\omega_1 = \Delta E$ or $\omega_2 = 2\Delta E$, respectively. Both fields are circularly polarized and the laser vectors rotate in the same direction. Within expectation, a ring in Fig. 8(a), representing the minimum probability, is embedded in the photoelectron wave function, which leads to the split of the momentum spectrum shown in Fig. 8(d). This split is due to the Rabi oscillation. In the middle column, the regular one-photon direct ionization gives rise to a circular symmetric distribution. The right column presents the results when the combined two-color field with $\phi = 0$ is used. The coherent sum of the one- and two-photon ionization pathways shows the interference structures, as shown in Figs. 8(c) and 8(f). The coherent summation makes the ring slightly vague. Different from Figs. 4(a) and 4(e) where no Rabi oscillation occurs, here we observed two minima in the ring in Fig. 8(c). Comparing to Fig. 4(a), the additional minimum is due to Rabi oscillations. These two minima are closely connected to two temporary largest two-photon ionization rates when the instantaneous populations in the first excited state of He^+ are maximum.

IV. CONCLUSIONS

In conclusion, He^+ in strong two-color XUV fields may undergo two ionization pathways if the XUV photon energies

are properly tuned. The first way is that He^+ is directly ionized by absorbing one high-energetic photon ω_2. The second way is that He^+ first absorbs one photon and jumps to the first excited state, and gets ionized by sequentially absorbing the second ω_1. In the indirect pathway, the electron may sit on the first excited state for some time before it is ionized by absorbing the second ω_1. The interference of these two pathways may enhance or suppress the ionization yield, depending on the electron emission direction and the relative phase of the two XUV fields. If the XUV pulse intensity (duration) with the frequency ω_1 is high (long) enough, Rabi oscillation will take place, which will make the two-pathway interference more complex. We demonstrate that intermediate states in photon ionization are very important. Reversely, it is promising to extract the phase information of bound states by analyzing the photoelectron spectra.

ACKNOWLEDGMENTS

This work was supported by NSF of China (Grants No. 11104180, No. 11175120, No. 11121504, No. 11322438, and No. 11574205) and the Fok Ying-Tong Education Foundation for Young Teachers in the Higher Education Institutions of China (Grant No. 131010).

[1] F. Krausz and M. Ivanov, Rev. Mod. Phys. **81**, 163 (2009).
[2] G. S. Hurst, M. G. Payne, S. D. Kramer, and J. P. Young, Rev. Mod. Phys. **51**, 767 (1979).
[3] J. Javanainen, J. H. Eberly, and Q. Su, Phys. Rev. A **38**, 3430 (1988).
[4] P. Agostini, F. Fabre, G. Mainfray, G. Petite, and N. K. Rahman, Phys. Rev. Lett. **42**, 1127 (1979).
[5] W. C. Wallace, M. G. Pullen, D. E. Laban, O. Ghafur, H. Xu, A. J. Palmer, G. F. Hanne, K. Bartschat, A. N. Grum-Grzhimailo, H. M. Quiney, I. V. Litvinyuk, R. T. Sang, and D. Kielpinski, New J. Phys. **15**, 033002 (2013).
[6] X. M. Tong, Z. X. Zhao, and C. D. Lin, Phys. Rev. A **66**, 033402 (2002).
[7] K. Y. Huang, Q. Z. Xia, and L. B. Fu, Phys. Rev. A **87**, 033415 (2013).
[8] O. Pedatzur, G. Orenstein, V. Serbinenko, H. Soifer, B. D. Bruner, A. J. Uzan, D. S. Brambila, A. G. Harvey, L. Torlina, F. Morales, O. Smirnova, and N. Dudovich, Nat. Phys. **11**, 815 (2015).
[9] W. Becker, X. J. Liu, P. J. Ho, and J. H. Eberly, Rev. Mod. Phys. **84**, 1011 (2012).
[10] P. B. Corkum, Phys. Today **64**, 36 (2011).
[11] M. W. Noel and C. R. Stroud, Jr., Phys. Rev. Lett. **75**, 1252 (1995).
[12] S. N. Yurchenko, S. Patchkovskii, I. V. Litvinyuk, P. B. Corkum, and G. L. Yudin, Phys. Rev. Lett. **93**, 223003 (2004).
[13] F. Lindner, M. G. Schätzel, H. Walther, A. Baltuška, E. Goulielmakis, F. Krausz, D. B. Milošević, D. Bauer, W. Becker, and G. G. Paulus, Phys. Rev. Lett. **95**, 040401 (2005).
[14] X. J. Liu, N. A. Cherepkov, S. K. Semenov, V. Kimberg, F. Gel'mukhanov G. Prūmper, T. Lischke, T. Tanaka, M. Hoshino, H. Tanaka, and K. Ueda, J. Phys. B **39**, 4801 (2006).
[15] L. Xin, H. C. Qin, W. Y. Wu, and F. He, Phys. Rev. A **92**, 063803 (2015).
[16] Th. Ergler, A. Rudenko, B. Feuerstein, K. Zrost, C. D. Schröter, R. Moshammer, and J. Ullrich, Phys. Rev. Lett. **97**, 193001 (2006).
[17] M. Meckel, D. Comtois, D. Zeidler, A. Staudte, D. Pavičić, H. C. Bandulet, H. Pépin, J. C. Kieffer, R. Dörner, D. M. Villeneuve, and P. B. Corkum, Science **320**, 1478 (2008).
[18] L. V. Keldysh, Sov. Phys. JETP **20**, 1307 (1965).
[19] J. L. Krause, K. J. Schafer, and K. C. Kulander, Phys. Rev. Lett. **68**, 3535 (1992).
[20] P. B. Corkum, Phys. Rev. Lett. **71**, 1994 (1993).
[21] B. Walker, B. Sheehy, L. F. DiMauro, P. Agostini, K. J. Schafer, and K. C. Kulander, Phys. Rev. Lett. **73**, 1227 (1994).
[22] C. Ruiz, L. Plaja, and L. Roso, Phys. Rev. Lett. **94**, 063002 (2005).
[23] P. Brumer and M. Shapiro, Chem. Phys. Lett. **126**, 541 (1986).
[24] S. T. Pratt, J. Chem. Phys. **104**, 5776 (1996).
[25] K. J. Yuan and A. D. Bandrauk, J. Mod. Opt. **60**, 1492 (2013).
[26] F. He, C. Ruiz, A. Becker, and U. Thumm, J. Phys. B **44**, 211001 (2011).
[27] P. Johnsson, J. Mauritsson, T. Remetter, A. L'Huillier, and K. J. Schafer, Phys. Rev. Lett. **99**, 233001 (2007).
[28] C. W. Hogle, X. M. Tong, L. Martin, M. M. Murnane, H. C. Kapteyn, and P. Ranitovic, Phys. Rev. Lett. **115**, 173004 (2015).
[29] M. Chini, B. Zhao, H. Wang, Y. Cheng, S. X. Hu, and Z. Chang, Phys. Rev. Lett. **109**, 073601 (2012).
[30] J. Mauritsson, T. Remetter, M. Swoboda, K. Klünder, A. L'Huillier, K. J. Schafer, O. Ghafur, F. Kelkensberg, W. Siu, P. Johnsson, M. J. J. Vrakking, I. Znakovskaya, T. Uphues, S. Zherebtsov, M. F. Kling, F. Lépine, E. Benedetti, F. Ferrari, G. Sansone, and M. Nisoli, Phys. Rev. Lett. **105**, 053001 (2010).
[31] R. Kosloff and D. Kosloff, J. Comput. Phys. **63**, 363 (1986).
[32] W. H. Press, S. A. Teukolsky, W. T. Vetterling, and B. P. Flannery, *Numerical Recipes* (Cambridge University Press, Cambridge, 1992).
[33] X. Xie, Phys. Rev. Lett. **114**, 173003 (2015).
[34] M. Richter, M. Kunitski, M. Schöffler, T. Jahnke, L. P. H. Schmidt, M. Li, Y. Liu, and R. Dörner, Phys. Rev. Lett. **114**, 143001 (2015).
[35] J. W. Geng, W. H. Xiong, X. R. Xiao, L. Y. Peng, and Q. Gong, Phys. Rev. Lett. **115**, 193001 (2015).
[36] X. Zheng, M. M. Liu, H. Xie, P. Ge, M. Li, and Y. Liu, Phys. Rev. A **92**, 053422 (2015).
[37] Z. Zeng, Y. Cheng, X. Song, R. Li, and Z. Xu, Phys. Rev. Lett. **98**, 203901 (2007).
[38] L. Y. Peng and A. F. Starace, Phys. Rev. A **76**, 043401 (2007).
[39] K. J. Yuan and A. D. Bandrauk, Phys. Rev. A **85**, 013413 (2012).
[40] H. Wang, M. Chini, S. Chen, C. H. Zhang, F. He, Y. Cheng, Y. Wu, U. Thumm, and Z. Chang, Phys. Rev. Lett. **105**, 143002 (2010).
[41] C. Ott, A. Kaldun, P. Raith, K. Meyer, M. Laux, J. Evers, C. H. Keitel, C. H. Greene, and T. Pfeifer, Science **340**, 716 (2013).

[42] A. S. Kheifets and I. A. Ivanov, Phys. Rev. Lett. **105**, 233002 (2010).
[43] I. A. Ivanov, Phys. Rev. A **83**, 023421 (2011).
[44] J. Su, H. Ni, A. Jaron-Becker, and A. Becker, Phys. Rev. Lett. **113**, 263002 (2014).
[45] C. A. Mancuso, D. D. Hickstein, P. Grychtol, R. Knut, O. Kfir, X. M. Tong, F. Dollar, D. Zusin, M. Gopalakrishnan, C. Gentry, E. Turgut, J. L. Ellis, M. C. Chen, A. Fleischer, O. Cohen, H. C. Kapteyn, and M. M. Murnane, Phys. Rev. A **91**, 031402 (2015).
[46] K. J. LaGattuta, Phys. Rev. A **47**, 1560 (1993).